*Laser and Particle Beams* (1996), *vol.* 14, *no.* 4, *pp.* 543–553
Printed in the United States of America



# Basic and applied atomic spectroscopy in high-field ion diode acceleration gaps

By J.E. BAILEY,* A.B. FILUK,* A.L. CARLSON,* D.J. JOHNSON,* P. LAKE,* E.J. McGUIRE,* T.A. MEHLHORN,* T.D. POINTON,* T.J. RENK,* W.A. STYGAR,* Y. MARON,** AND E. STAMBULCHIK**

*Sandia National Laboratories, Albuquerque, NM 87185
**Weizmann Institute of Science, Rehovot, Israel, 76100

(Received 15 December 1995; Revised 20 April 1996; Accepted 1 June 1996)

Achieving inertial confinement fusion using a light-ion-beam driver requires continued improvement in understanding ion diode physics. The power delivered to a light-ion beam target is strongly influenced by the evolution of the charge-particle distributions across the ion beam acceleration gap. Our strategy is to determine this evolution from time- and space-resolved measurements of the electric field using Stark-shifted line emission. In addition to diode physics, the unique high-field (~10 MV/cm, ~6T) conditions in present experiments offer the possibility to advance basic atomic physics, for example by measuring field ionization rates for tightly bound low-principal-quantum-number levels. In fact, extension of atomic physics into the high-field regime is required for accurate interpretation of diode physics measurements. This paper describes progress in ion diode physics and basic atomic physics, obtained with visible-light atomic spectroscopy measurements in the ~20 TW Particle Beam Fusion Accelerator II ion diode.

## 1. Introduction

Pulsed-power light-ion-beam diodes are a promising candidate driver for achieving inertial confinement fusion (VanDevender & Cook 1986). The major obstacle to this goal is inadequate understanding of the underlying physics in the ion diode that transfers electrical power to the ion beam. This motivates atomic spectroscopy measurements aimed at improving understanding of the complex phenomena existing in the ion diode acceleration gap. The high electric fields (~10 MV/cm) generated in the gap both enable and demand the extension of experimental atomic physics into a new regime. This paper describes our application of atomic spectroscopy to ion diode plasma physics issues, with an emphasis on the atomic physics required to understand the results. In addition, we describe preliminary experiments that illustrate the potential of using data from these devices for basic atomic physics.

The ion-beam power delivered to the target is strongly influenced by the charged particle dynamics in the anode-cathode (AK) gap. The space charge in the gap limits the ion current density according to the Child–Langmuir relation, $J_{CL} = k(Ze/m)^{1/2}V^{3/2}/d^2$, where $k$ is a constant, $Ze/m$ is the charge-to-mass ratio, and $V$ is the voltage. The dimension of the $AK$ gap $d$ is determined by the distance between the physical anode (or anode plasma) and the virtual cathode formed by electrons confined in the applied magnetic field. An electron cloud filling the region between the virtual cathode and the anode is known to exist (Bailey *et al.* 1995). However, the charged-particle dynamics are uncertain at present,

 0263-0346/96 $11.00 + .10

despite significant theoretical studies of this complex phenomenon (Slutz *et al.* 1986; Desjarlais 1987). The electrons populating the region between the virtual cathode and the anode are most likely due to cross-field flow and injection of electrons into the middle of the diode gap from the magnetically insulated transmission lines. These electrons effectively cancel some of the ion space charge and enhance the ion current above the nominal Child limit. This configuration—an electron cloud with an ion beam streaming through it—is susceptible to a variety of instabilities (Desjarlais *et al.* 1991; Slutz & Johnson 1992; Pointon *et al.* 1994; Krall 1994). These instabilities can influence the distribution of the electrons across the AK gap because they enable rapid cross-field flow. Nonuniformities can also influence electron transport across the field lines. In addition, the nonradial electric fields resulting from instabilities or nonuniformities can deflect the ions and contribute to the ion-beam divergence. Understanding the charged particle distributions is therefore of fundamental importance as we seek to increase the ion beam brightness.

## 2. Experimental methods

The experiments described in this paper were performed using a cylindrically symmetric applied-magnetic-field ion diode (Johnson *et al.* 1982; Mehlhorn *et al.* 1994). The Particle Beam Fusion Accelerator II (PBFA II) supplied a 20-TW, ~20-ns, 10-MV power pulse through conical magnetically insulated transmission lines connected to the top and bottom of the diode (figure 1). The ion beam is accelerated radially inward from an approximately cylindrical anode toward a target placed on the axis. An approximately 3-T magnetic field, applied parallel to the anode, insulates the AK gap against electron losses.

The primary diagnostic for the AK gap charged-particle dynamics is visible-light atomic spectroscopy (Bailey *et al.* 1995). Other methods such as Thompson scattering or inter-

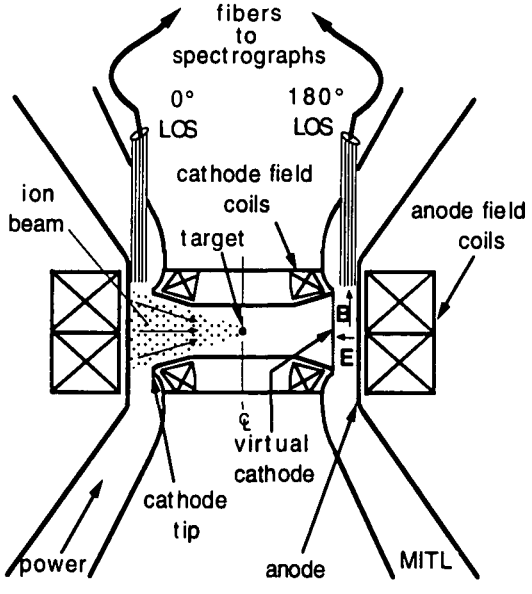


FIGURE 1. Diagram of the PBFA II ion diode. The diode is cylindrically symmetric about the center line CL. MITL refers to the biconic magnetically insulated transmission lines that couple power from the accelerator to the diode. Spectroscopic line of sight (LOS) bundles are shown located in two azimuths at 0° and 180°, with each bundle measuring the emission from 3–7 radial positions across the AK gap.

https://doi.org/10.1017/S0263034600010260 Published online by Cambridge University Press

ferometry are exceedingly difficult due to the need to measure relatively low densities ($10^{12} - 10^{13}$ cm$^{-3}$) with ~1-ns time resolution and ~1-mm spatial resolution in the harsh pulsed-power environment. The strategy we follow is similar to the method developed by Maron *et al.* (1986, 1987). We measure the magnitude of the electric field $|E|(r,\phi,t)$ from Stark-shifted line emission and determine the charged-particle dynamics from $\nabla \cdot E = 4\pi\rho = 4\pi e(Zn_i - n_e)$, where $e$ is the electron charge and $Ze$ is the ion charge. The net charge density $\rho$ is determined by fitting a curve to $E$ and differentiating, under the assumption that $E = E_r$. The ion velocity is given by $v_i^2(r) = 2Ze/m_i \int E\,dr$ and we determine the ion density from $n_i(r) = J_i/Zev_i(r)$, where $J_i$ is the measured ion current density. The electron density $n_e$ is obtained by subtracting the net charge density from the ion density $n_i$.

The visible spectroscopy diagnostic system is described by Bailey *et al.* (1990, 1994). We collect light from approximately cylindrical 2-mm-diameter lines of sight aligned parallel to the anode. Multiple lines of sight are used to obtain radial and azimuthal spatial resolution, where the radially resolved measurements provide a profile across the AK gap and the azimuthal measurements determine the degree of cylindrical uniformity (see figure 1). The configuration shown in figure 1 is used to determine the global uniformity on opposite sides of the diode, while a second configuration (not shown) with 2–10-mm azimuthal spacing measures the uniformity over a small azimuthal sector. The light is transported in fiber optics to remote streaked spectrographs for recording with ~1 ns time resolution. A multiplexing technique enables time-resolved spectra with ~50 Å range and 1.5 Å resolution to be recorded simultaneously from 18 different spatial locations. The relative spacing is accurate to ±0.2 mm and the absolute accuracy of the line of sight bundle relative to the anode surface is ±0.5 mm. The timing between spectra is accurate to ±0.4 ns and the timing accuracy relative to the electrically recorded diagnostics is ±2 ns. An extensive suite of diagnostics measures the ion beam parameters (Leeper *et al.* 1988). The ion current and current density are measured with an array of *dB/dt* loops and Faraday cups, respectively. The beam kinetic energy is determined with a magnetic spectrometer that observes beam ions that are Rutherford-scattered from thin Au foil targets placed in the beam path.

Most measurements to date have relied on Stark-shifted 2*s*-2*p* emission from lithium neutrals. These neutrals are launched into the gap when a small fraction of the lithium ions charge exchange in a thin dense contaminant layer near the anode. We determine the neutral velocity by measuring the propagation of the 2*s*-2*p* intensity into the gap, taking into account the radiative decay and other factors that influence the emission intensity. The charge-exchange origin of the Li neutrals impacts the electric field measurements because the Li neutrals acquire a high velocity transverse to the acceleration direction, due to the ion beam source divergence (the details of the charge exchange and the determination of ion beam source divergence from the neutral Doppler broadening will be discussed in a forthcoming publication). This high transverse velocity results in large Doppler broadening (typically 10–15 Å) that prevents resolution of the individual Stark–Zeeman line components. In addition, measurements on the cathode side of the gap are not possible until neutrals arrive there, typically ~10–15 ns into the pulse. Nevertheless, the Li I charge-exchange neutral emission is convenient, it provides good accuracy without disturbing the normal diode operation, and measurements with neutrals provide brighter visible light emission intensities than ion emission measurements. Also, note that the Doppler broadening of the Li neutral emission is relatively small in comparison to self-emission measurements from ions, since the ions are likely to acquire more and more divergence as they cross the gap, while the divergence of the charge-exchange neutrals is set by the beam divergence near the anode at the location of the charge-exchange event. We typically analyze 15–20 lineouts from each spectrum, averaging over 4-ns intervals to improve the signal-to-noise ratio.

A single Gaussian is fit to each spectral line, with a wavelength uncertainty determined using the fluctuation levels of the entire spectrum (Coldwell & Bamford 1991). The shift is measured relative to the zero-field wavelength established using emission from after the power pulse (when the electric field is zero). The procedure determines the Stark shifts with a typical uncertainty ±0.2–0.4 Å, compared to ~6 Å maximum shifts.

The spectral data provides the Stark shift as a function of time and space. The interpretation of this data requires calculations of the Stark–Zeeman line emission pattern as a function of $|E|$ and $|B|$, for values of $|E|$ that are higher than any previous terrestrial Stark shift measurement. Independent calculations were performed at Sandia (McGuire 1995) and at the Weizmann Institute (Stambulchik & Maron 1994) to improve confidence in the results. Both calculations use direct diagonalization of the Hamiltonian without invoking a perturbation approach. The Zeeman and Stark effects are treated self-consistently and the effects of high-lying levels are included. The Weizmann Institute calculations also include level shifts due to interaction with continuum states. The calculations agree to ~1% with available published data (Hunter *et al.* 1991; Windholz *et al.* 1992) that extend up to ~0.4 MV/cm. A comparison of the two calculations for the Li I 2*s*-2*p* transition using $B = 6$ T and $E = 0$–11 MV/cm is shown in figure 2, where the centroid of the emission pattern is averaged over all observation directions (in actual data analysis we take the directions of the electric and magnetic fields and the line of sight into account). Note that the shift is to the blue so that larger shifts correspond to shorter wavelengths. The impact of the magnetic field strength on the interpretation of the experiments reported here is negligible because the high electric field dominates the centroid shift and the large Doppler broadening prevents observation of the individual line components. A shift assuming a quadratic dependence on $E$ is also shown in figure 2. The shift in both calculations is approximately quadratic in $E$ for fields up to about 5 MV/cm, but at higher fields the calculated shifts deviate from the quadratic curve. At any given shift, the fields determined from the two calculations agree to better than ±5% for fields up to 10 MV/cm. This uncertainty is not included in the error bars presented below. The differences between the calculations at fields above 10 MV/cm are currently under investigation.

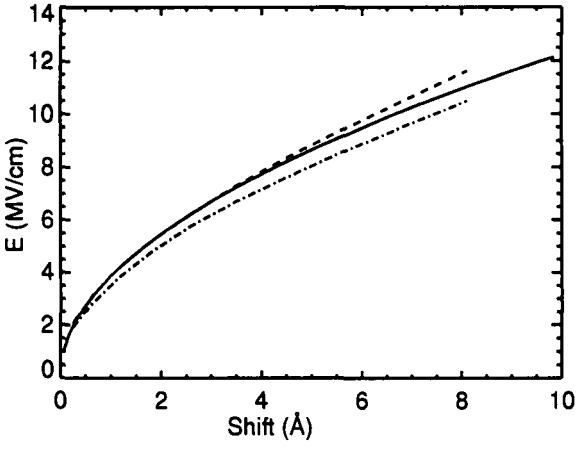


FIGURE 2. Electric field as a function of the Stark–Zeeman emission pattern centroid wavelength shift for the Li I 2*s*-2*p* transition at $B = 6$ *T*. The dashed curve is from Stambulchik and Maron (1994) and the dot-dash curve is from McGuire (1995). The solid curve represents the quadratic relationship, shift (Å) ~ $E(\text{MV/cm})^2/15$, illustrating the departure of the shift from the quadratic approximation at fields above about 5 MV/cm.

https://doi.org/10.1017/S0263034600010260 Published online by Cambridge University Press

## 3. Applications of atomic spectroscopy to diode physics

A temporal sequence of electric field profiles measured from Stark-shifted Li I 2*s*-2*p* emission in a single PBFA II experiment is shown in figure 3. The AK gap in this experiment was 18 mm. The first measurement at 46 ns corresponds to the onset of ion current. The diode physics aspects of these results are described in Bailey *et al.* (1995). The electric field routinely exceeds 10 MV/cm, an order of magnitude higher than any previous laboratory Stark-shift emission measurement. The field measured near the anode surface is 9–10 MV/cm, in contrast to the zero field expected for a space-charge-limited plasma ion source. This result is consistent with a recent theoretical hypothesis (Green 1995; Stinnett *et al.* 1992) that the LiF ion source produces Li ions via electron-assisted field desorption. The almost-flat electric field profile near the anode at peak ion power (62 ns) implies that there is a ~2–3-mm-thick, zero-net-charge region near the anode, in contrast to the positive net charge suggested by the simulations. About 10 mm from the anode, the electric field profile reverses its slope from negative to positive, implying a region with localized positive net charge in the middle of the gap. We emphasize, however, that these results are obtained by assuming uniform conditions along the line of sight. The effect of possible nonuniformities on the conclusions is under investigation. Azimuthal asymmetries between the measurements performed on opposite sides of the diode persist over much of the pulse, indicating that $E \times B$ drifting electrons are unable to cancel them. These results suggest that

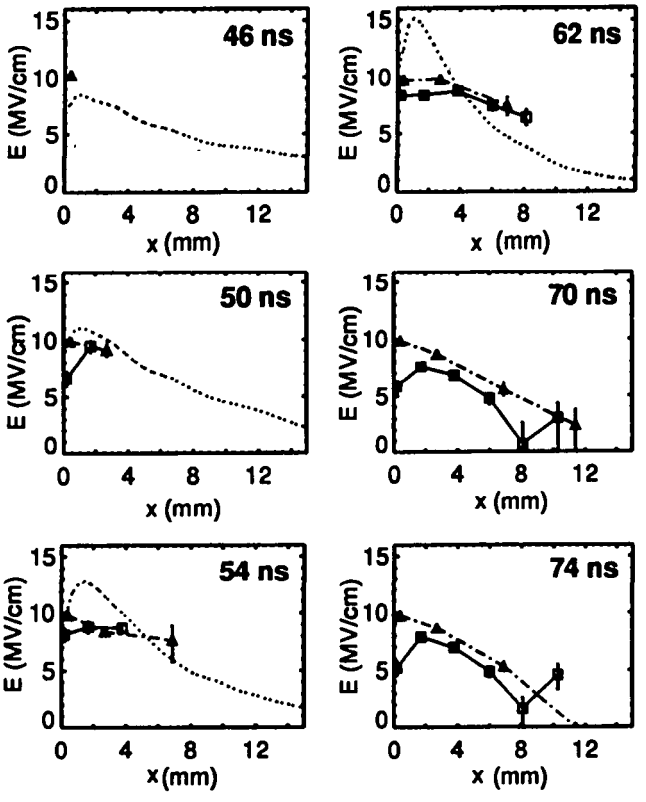


FIGURE 3. Electric field evolution as a function of $x$, the radial distance away from the anode. The squares and triangles are measurements from a PBFA II experiment at the 180° and 0° azimuths, respectively. The dashed curve is a QUICKSILVER simulation result (Pointon *et al.* 1994).

https://doi.org/10.1017/S0263034600010260 Published online by Cambridge University Press

improvements are required in both experiments and simulations to understand the power coupling efficiency and divergence.

In the cylindrical barrel-diode geometry, the electric field that accelerates the ions toward the target is primarily radial. However, nonradial field components can arise from electromagnetic instabilities and/or nonuniformities in the ion emission, cathode plasma, or virtual cathode electron cloud. These nonradial components deflect the ion beam and add to its divergence as it crosses the AK gap, effectively decreasing the beam power density irradiating the target. One method for determining which mechanisms for divergence growth are most important is to measure the growth of beam divergence as the beam is accelerated, for example by measuring the Doppler broadening of the lithium ion line emission perpendicular to the radial ion acceleration direction. This is extremely difficult for the present conditions because of the high radial beam velocities, the low beam ion density, and the low fraction of the Li II ions that populate the excited states. An alternative using emission from dopant ions, such as Ba II, is described below. As another alternative, we are attempting to directly determine the nonradial electric field components responsible for the divergence growth from our measurements of $|E|$. This may in fact be preferable to measuring the divergence itself since our goal is to identify and eliminate the divergence-inducing mechanism.

The method for measuring the nonradial field component $E_\phi(r,\phi,t)$ is illustrated in figure 4. We measure the magnitude of the electric field vector $|E| = [E_r^2 + E_\phi^2 + E_z^2]^{1/2}$ as a function of time on a rectangular array of spectroscopic lines of sight. Each line of sight is represented by a solid circle in figure 4. The potential at each azimuth $V_A$ or $V_B$ as a function of radius is obtained by integration of the field, using the approximation that $E \sim E_r$. With this method, we obtain the potential for adjacent azimuths as a function of radius and time. The azimuthal component of the electric field $E_\phi$ is then approximately the potential difference between two azimuths $V_{AB}$, divided by the azimuthal distance between them $\delta$, using the fact that the line integral of $E$ around the dotted path is zero (estimates for the $dB/dt$ term in this equation indicate that this term is negligible). The chal-

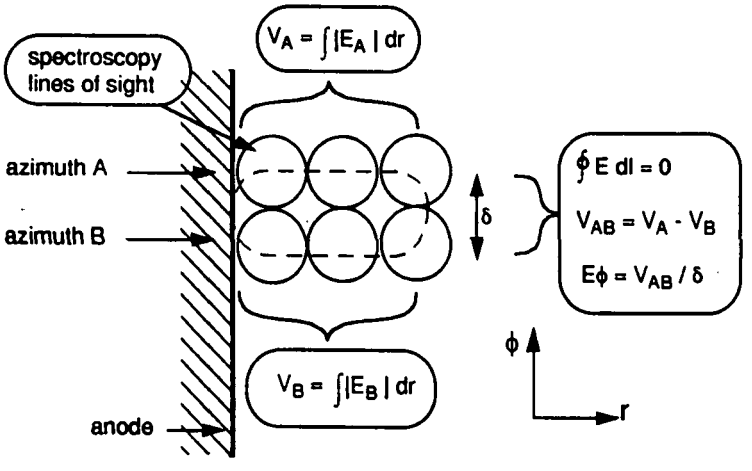


FIGURE 4. Top view of the diode AK gap illustrating the method used to determine the nonradial electric fields from the Stark shift measurements. The circles represent individual spectroscopic lines of sight that are approximately 2 mm in diameter. The dashed curve illustrates the path for the line integral. In actual experiments, a larger array of points (up to 18 total) is used to obtain more complete measurements of the radial and azimuthal dependence.

https://doi.org/10.1017/S0263034600010260 Published online by Cambridge University Press

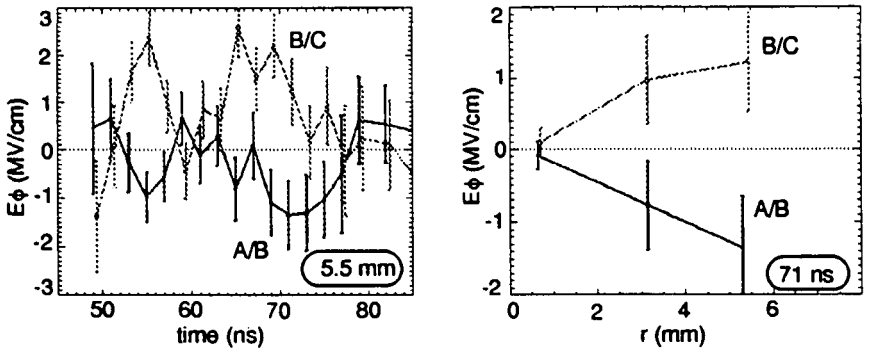


FIGURE 5. Preliminary measurements of azimuthal components of the electric field obtained using a line of sight arrangement similar to that shown in figure 4, but with an additional row of lines of sight at a third azimuth. The curves labeled A/B refer to one pair of azimuths and the curves labeled B/C refer to the other pair. Ion current onset in this experiment was at 41 ns. The time history on the left corresponds to 5.5 mm from the anode surface and the spatial plot on the right corresponds to $t = 71$ ns.

lenge in applying this method is that the differences in $|E|$ are of order 10%, requiring that the uncertainty in $|E|$ be less than about 5% to arrive at statistically significant values for $E_\phi$. The typical uncertainty in our present experiments ranges over ±2–6% (at $1\sigma$). This is adequate, but the accuracy of $E_\phi$ would clearly benefit from reduced uncertainties. Preliminary results for $E_\phi(r,t)$ are shown in figure 5. The azimuthal field component grows with distance from the anode and it fluctuates on a 2–8 ns time scale. If confirmed, the measured $E_\phi$ within 5.5 mm of the anode is sufficient to cause ~25 mrad of beam deflection (averaged over the first 1/2–2/3 of the power pulse), comparable to the 25–35 mrad measured at the target on axis. Work is in progress to measure the radial and azimuthal extent of $E_\phi$ over larger radial and azimuthal distances to help identify its origin.

## 4. Basic atomic physics

Additional aspects of atomic physics and diode physics can be explored by adding impurity dopants to the anode. In one such experiment, $BaF_2$ and LiF were coevaporated onto the substrate in an approximately 1:1 molecular ratio. The primary motivations for adding $BaF_2$ to the anode were to provide a direct measurement of ion divergence and to enable Zeeman measurements of the magnetic field. As mentioned above, the lithium ion beam divergence is difficult to measure directly. Measurements of Ba II Doppler broadening are straightforward in comparison to Li II measurements, because the high Ba ion mass makes the Ba ion density relatively high and the easily excited resonance transition lies in the visible regime. In addition, the Ba II Doppler broadening is expected to be smaller than for the Li I charge-exchange neutrals. This may enable measurements of the magnetic field profile from the Stark–Zeeman pattern (Maron *et al.* 1989).

These diode physics results will be discussed elsewhere. Here, we only point out that simultaneous measurements of the electric field from Ba II and Li I emission provide a useful cross-check of the Stark pattern calculations. A temporal sequence of lineouts measuring the Ba II $6s^2S_{1/2}$-$6p^2P_{1/2}$ transition are shown in figure 6. This transition is split into two components, one appearing at the zero-field wavelength and one that is Stark shifted. The intensity of the unshifted component relative to the shifted feature grows in time. The appearance of a Stark-shifted component verifies that it is indeed possible to

https://doi.org/10.1017/S0263034600010260 Published online by Cambridge University Press

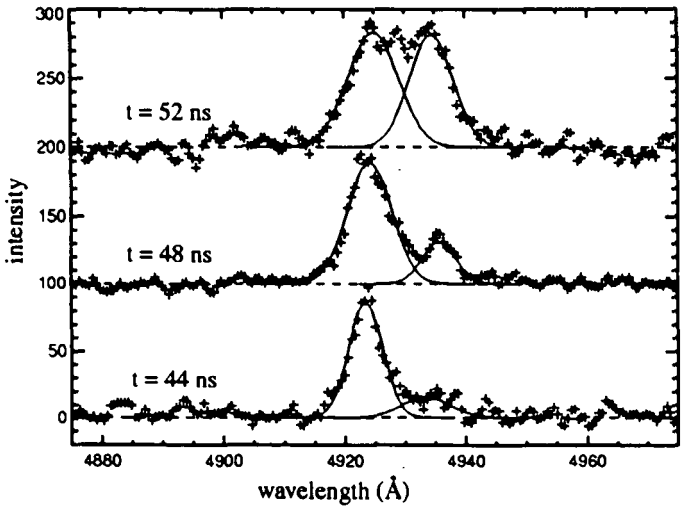


FIGURE 6. A temporal sequence of lineouts for the BaII $6s\,^2S_{1/2}$-$6p\,^2P_{1/2}$ transition, measured adjacent to the PBFA II anode. Each successive time step is displaced by 100 intensity units to facilitate viewing. Gaussian fits to the peaks (solid curves) obtained with the ROBFIT code are superimposed on the data (plus signs). The unshifted (zero field) wavelength is 4934.1 Å.

observe Ba II emission as the ions are accelerated across the gap. Interpretation of the fact that both shifted and unshifted light are observed simultaneously is in progress, but it appears to be consistent with acceleration of barium ions from both field-threshold-emission regions (as for LiF) and from plasmas. This complex situation presently limits the comparison of electric field determined from Ba II and Li I emission to early times when the Ba II emission is completely shifted. At this time the fields agree to within 10%. Better agreement cannot be expected, because in the present experiment the Ba II and Li I emissions were collected with lines of sight located at the same radial distance from the anode, but at adjacent azimuths separated by 2 mm. Data described above shows that differences of about 10% in $|E|$ can exist over this azimuthal separation. We plan to perform a more stringent test of these Stark pattern calculations by collecting light in a single line of sight and splitting it into two streaked spectrographs. This should enable a cross-comparison of the Li I and Ba II results to within approximately ±5%.

The extension of basic atomic physics into the 10-MV/cm regime is illustrated by measurements of the Li I $2p$-$3d$ transition. Spectroscopic studies of field ionization for tightly bound low-principal-quantum-number levels such as the $3d$ require quasistatic fields exceeding ~3 MV/cm, produced over a sufficiently large region that emission or absorption lines can be observed. The conditions in the PBFA II acceleration gap meet these requirements, making such experiments possible for the first time. The analysis of the data described below is still in progress. Nevertheless, they serve to illustrate the interesting possibilities for atomic physics measurements in the high-field regime.

Streaked spectral emission measured 9 mm from the PBFA II anode is shown in figure 7. We observe transitions from Li I as well as from H I and Na I impurities (the sodium was added intentionally for diagnostic development). In this experiment we first observe shifted Li I $2s$-$2p$ emission at ~56 ns, simultaneous with the onset of ion current. The Li I $2p$-$3d$ emission is not observed until ~78 ns and, when it first appears, it is split into red- and blue-shifted components. Interpretation of these data requires an understanding of the

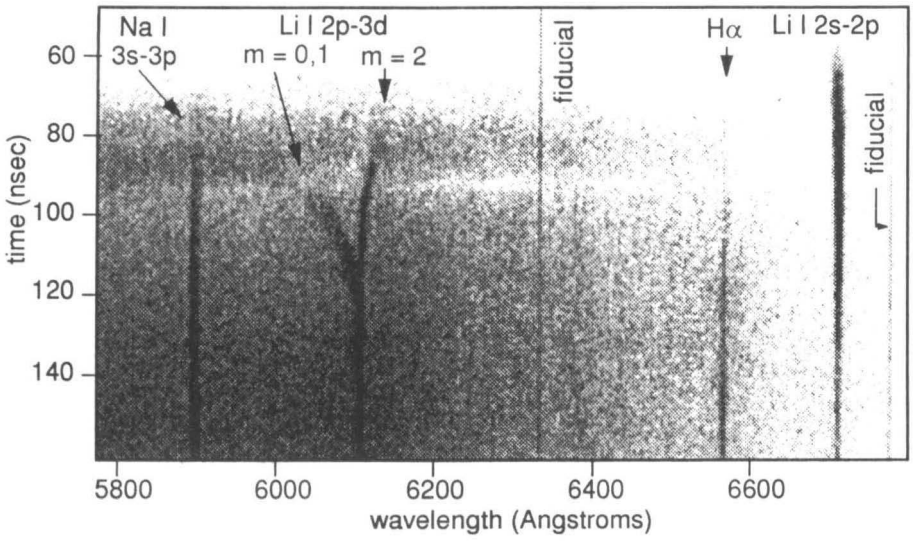


FIGURE 7. Streaked spectrum measuring Li I $2p$-$3d$ transition 9 mm from the PBFA II anode surface. The $2p$-$3d$ emission arises about 25 ns after the onset of lithium ion beam current.

various population and depopulation rates, as well as accurate calculations of the Stark–Zeeman patterns. The $3d$ level is populated in the same charge exchange events that populate the $2p$ level, as well as by ion impact excitation from the $2p$ level. The dominant deexcitation mechanisms are expected to be field ionization and radiative decay. Prior measurements of the state-selective charge exchange cross section (Odom *et al.* 1976) indicate significant $3d$ population should be present early in the power pulse. The fact that the $2p$-$3d$ emission is not observed until the end of pulse is almost certainly because the $3d$ rapidly field ionizes under the 5–10-MV/cm field. This is consistent with previous detailed calculations of the field ionization rate (Themelis & Nicolaides 1994) and expectations based on semiclassical approximations.

When the $2p$-$3d$ does appear, it is split into red-shifted and blue-shifted components. The red-shifted component arises from the $3d\, m_L = 2$ state and the blue-shifted component is a superposition of transitions originating from the $3d\, m_L = 0,1$ states. The $m_L = 2$ transition is red-shifted, and is less strongly perturbed, because the selection rules prohibit the $3p$ level from perturbing the $3d\, m_L = 2$ state. The red-shifted feature appears first. The delayed appearance of the blue-shifted feature is because this component has a lower threshold for field ionization and it is more strongly shifted once it does appear. The larger Stark shift of the $m_L = 0, 1$ states and the existence of even small electric field variations along the line of sight tend to smear out the blue-shifted transitions into a broad line, making it more difficult to observe above the continuum. The field measured from the red-shifted feature is consistent with the field obtained from the $2s$-$2p$ transition. While this agreement is satisfying, it does not represent a stringent test of the Stark pattern calculations because the uncertainty associated with measuring the field from the $2s$-$2p$ transition grows as the field shrinks below about 3 MV/cm.

The $m_L = 2$ transition first appears at a field of ~3.7–3.9 MV/cm. This is roughly consistent with theoretical predictions that this state field ionizes at $E \sim 4.7$ MV/cm, but further analysis of the population mechanisms is required. At present it appears that the $3d$ emission we observe does not arise from charge-exchange neutrals born at the anode. The

https://doi.org/10.1017/S0263034600010260 Published online by Cambridge University Press

velocity of the charge-exchange neutrals during the early part of the pulse is determined in other experiments using measurements of the time-dependent Li I $2s$-$2p$ emission intensity on multiple lines of sight at different distances away from the anode. This velocity is typically ~50 cm/$\mu$s, corresponding to a ~15–20 ns time of flight between the anode and the spectroscopic line of sight located 9 mm away. This implies that if the origin of the Li I $2p$-$3d$ emission was charge-exchange neutrals, they survived the high fields existing in the AK gap during the ~15–20 ns prior to the initial observation of the $2p$-$3d$ emission. Calculations of the field ionization (Themelis & Nicolaides 1994) indicate that this is unlikely. Excitation from the Li I $2p$ state by Li ion impact excitation is also under investigation (electron impact excitation is considered unlikely because of the relatively low electron densities in the diode gap). The elapsed time between the field dropping below ~ 4.7 MV/cm (where fast field ionization is expected) and reaching the 3.7–3.9-MV/cm field (where the transition is observed) is about 3–5 ns. The key question to evaluate for the ion impact excitation hypothesis is whether this is long enough to produce sufficient $3d\, m_L = 2$ population to account for the observed intensity, given the measured ion current density and $2p$ population density. A similar analysis can be applied to the $3d\, m_L = 0$, 1 states. Resolution of these issues may enable testing of theoretical predictions for the field ionization rates.

## 5. Conclusion

Measurements of Stark-shifted emission clearly provide new insight into the complex plasma physics in ion diode acceleration gaps. In particular, these measurements enable comparisons of the 3D electromagnetic simulations that are used to predict diode operation with detailed measurements for the first time. Interpretation of the measurements requires accurate calculations of the line emission patterns under ~ 10-MV/cm electric fields and 3- to 6-T magnetic fields. In addition, the high field routinely produced on PBFA II invites basic atomic physics measurements for many species that were previously impossible.

The above advances in plasma and atomic physics were made in spite of some disadvantages to our present method that relies on naturally occurring self-emission from the AK gap. For example, we integrate along a line of sight that may include variations in the field being measured, and measurements on the cathode side of the gap are inhibited because of the time that elapses before the charge-exchange neutrals to arrive there. In addition, while the Li I $2s$-$2p$ transition is admirably suited to measuring 3- to 10-MV/cm fields, it is less sensitive to the lower fields characteristic of the virtual cathode location. In future experiments we plan to remove these difficulties by using laser-induced fluorescence to probe a neutral vapor or ions introduced into the diode gap prior to the arrival of the power pulse. This should enable more definitive measurements, leading to more rapid understanding of the plasma physics in the AK gap and to new possibilities for basic atomic physics.

## Acknowledgments

The authors thank the PBFA II operations crew, P.M. Baca, and D.F. Wenger for technical assistance. We are also grateful to S.A. Slutz, T.R. Lockner, M.P. Desjarlais, and T. Nash for many useful discussions and to D.L. Cook, R.J. Leeper, and J.P. Quintenz for continuous support and encouragement. This work was supported by the U.S. Department of Energy under contract No. DE-AC04-94AL85000.

## REFERENCES

Bailey, J. *et al.* 1990 *Rev. Sci. Instrum.* **61**, 3075.

Bailey, J. *et al.* 1994 (IEEE Report No. 94CH3465-2, 1994).

BAILEY, J. *et al.* 1995 *Phys. Rev. Lett.* **74**, 1771.

COLDWELL, R.L. & BAMFORD G.J. 1991 *The Theory and Operation of Spectral Analysis USing ROBFIT* (AIP, New York).

DESJARLAIS 1987 *Phys. Rev. Lett.* **59**, 2295.

DESJARLAIS *et al.* 1991 *Phys. Rev. Lett.* **67**, 3094.

GREEN, T.A. 1995 Sandia Report SAND95-1794.

HUNTER, L.R. *et al.* 1991 *Phys. Rev. A* **44**, 6140.

JOHNSON, D.J., *et al.* 1982 *J. Appl. Phys.* **53**, 4579.

KRALL, N.A. 1994 *Phys. Plasmas* **1**, 2371.

LEEPER, R.J. *et al.* 1988 *Rev. Sci. Instrum.* **59**, 1860.

MARON Y. *et al.* 1986 *Phys. Rev. Lett.* **57**, 699.

MARON, Y. *et al.* 1987 *Phys. Rev. A* **36**, 2818.

MARON, Y. *et al.* 1989 *Phys. Rev. A* **39**, 5856.

MEHLHORN, T.A. *et al.* 1994 NTIS Report #PB95-144317.

MCGUIRE, G. 1995 (to be published).

ODOM, R. *et al.* 1976 *Phys. Rev. A* **14**, 965.

POINTON, T.D. *et al.* 1994 *Phys. Plasmas* **1**, 429.

SLUTZ, S.A. *et al.* 1986 *J. Appl. Phys.* **59**, 11.

SLUTZ, S.A. & JOHNSON, W.A. 1992. *Phys. Fluids B* **4**, 1349.

STAMBULCHIK, E. & MARON, Y. 1994. Weizmann Institute of Science Report No. WIS-90/40/Sept.-PH (unpublished).

STINNETT, R.W. *et al.* 1992 NTIS Report No. PB92-206168.

THEMELIS, S.I. & NICOLAIDES, C.A. 1994 *Phys. Rev. A.* **51**, 2801.

WINDHOLZ, L. *et al.* 1992 *Phys. Rev. A*, 5812.

VANDEVENDER, J.P. & COOK, D.L. 1986 *Science* **232**, 801.